IEEE Photonics Journal
An IEEE Photonics Society Publication

Localized Field Enhancements in Guided and Defect Modes of a Periodic Slot Waveguide

Volume 3, Number 6, December 2011

Judson D. Ryckman, Student Member, IEEE
Sharon M. Weiss, Member, IEEE

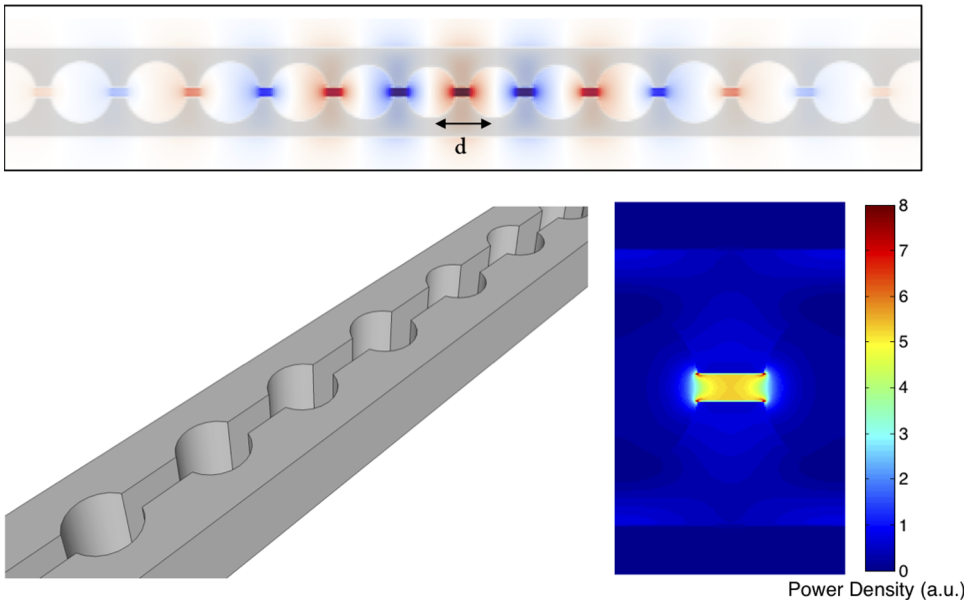

DOI: 10.1109/JPHOT.2011.2170966
1943-0655/$26.00 ©2011 IEEE

IEEE photonics SOCIETY

IEEE

Localized Field Enhancements in Guided and Defect Modes of a Periodic Slot Waveguide

Judson D. Ryckman, *Student Member, IEEE*, and Sharon M. Weiss, *Member, IEEE*

Department of Electrical Engineering and Computer Science, Vanderbilt University, Nashville, TN 37235 USA

DOI: 10.1109/JPHOT.2011.2170966
1943-0655/$26.00 ©2011 IEEE

Manuscript received September 23, 2011; accepted September 30, 2011. Date of publication October 10, 2011; date of current version November 1, 2011. This work was supported in part by the Air Force Office of Scientific Research under Grant FA9550-10-1-0366. This paper has supplementary downloadable material available at http://ieeexplore.ieee.org. provided by the authors. Corresponding author: J. D. Ryckman (e-mail: j.ryckman@vanderbilt.edu).

Abstract: We present a periodic slot waveguide for achieving enhanced light–matter interaction that provides significant localized field and power density enhancements over traditional slot waveguides. The basic structure is based on a slot waveguide with 1-D periodic holes. The slot effect provides strong field enhancement and subwavelength confinement, and the periodicity of the structure is exploited to locally magnify or "pinch" the electric field distribution, resulting in additional enhancements. Characteristics of the modes presented by this structure are examined by finite-difference time-domain (FDTD) modeling. Distinct optical gradients and localized $|E|^2$ enhancements, which are up to $\sim$4–5 times greater than comparable slot waveguides, can be achieved. Potential application of the periodic slot waveguide structure to fields, including optical manipulation, sensing, and nonlinear or active material integration, is discussed.

Index Terms: Nanophotonics, optical waveguides, optical resonators, photonic crystals.

1. Introduction

The slot waveguide has emerged as a useful tool within the growing suite of photonic components for achieving enhanced light–matter interactions due to its strong subwavelength confinement, enhanced field-intensity, low effective index, and large field overlap with void/cladding materials [1]. The distinct properties of the slot waveguide have led to advances in a wide variety of applications, including sensing [2]–[5], nano-optomechanics [6], [7], nonlinear effects [8]–[13], optical modulation [11]–[13], and optical manipulation [14]–[16]. Similarly, photonic crystals have gained significant attention across a breadth of applications due to their ability to enhance light–matter interactions by manipulating light in one, two, and three dimensions [17].

There is great potential in combining the photonic crystal and slot platforms to obtain superior characteristics within a single device structure. Indeed, recent works have theoretically investigated embedding a slot into 1-D photonic crystals, such as in a nanocavity to achieve ultralow mode volumes [18], [19], or in a coupled resonator configuration to obtain slow light effects [20]. In addition, several studies have investigated incorporating slots into the high-Q cavities of 2-D photonic crystal slab structures [5], [6], [13], [21], [22]. All of these demonstrations have sought to enhance the local field intensity and improve light–matter interaction by either trapping light in a slotted resonator or slowing-light down in a slotted photonic crystal waveguide. However, few of

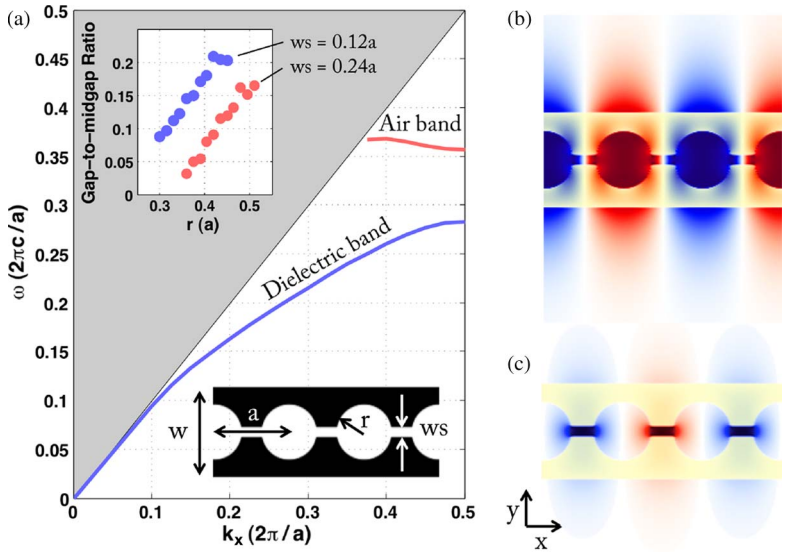

Fig. 1. (a) Band structure of a pinch waveguide with $r = 0.42a$, $w = 1.2a$, and slot width $ws = 0.12a$. Inset reveals the gap-to-midgap ratio as a function of hole radius size. Note that the gray shaded region represents the light cone above which radiation modes exist with a continuous spectrum. (b) Ey field distribution for a guided mode in the air band. (c) Ey field distribution for a guided mode in the dielectric band.

these works specifically investigate the strong field confinement and localized enhancements that can be achieved in the photonic crystal slot platform.

Here, we demonstrate that incorporating 1-D periodicity into the slot waveguide structure can be exploited to significantly redistribute the fields of both guided and defect modes, resulting in distinct optical gradients and localized field enhancements that exceed those of traditional slot or photonic crystal structures. The basic structure is highly tunable and can be readily integrated into the suite of existing nanophotonic components. We refer to this novel waveguide structure as the "*pinch waveguide*."

2. Finite-Difference Time-Domain Simulation of Guided Modes

2.1. Bands and Field Properties

The pinch waveguide structure consists of a traditional slot waveguide superimposed with air (or low index) holes periodically arranged at every interval *a* along the length of the waveguide. For an appropriate range of parameters, this structure exhibits a photonic bandgap (PBG), which prevents a set of frequencies $\{\omega_1, \omega_2\}$ from guiding. Outside of the PBG, there are various distinct bands, or eigenmodes, where guiding is possible.

To examine the modal characteristics of the pinch waveguide structure, simulations were performed using the 2-D finite-difference time-domain (FDTD) method [23], combined with harmonic analysis techniques [24], in a freely available software package [25]. Unless otherwise noted, all simulations are performed using normalized units with a grid resolution of $a/144$ and subpixel averaging enabled to improve accuracy [26].

Fig. 1(a) presents the proposed waveguide geometry and the band structure for an example design with a high dielectric contrast, with $\varepsilon_1 = 13$, $\varepsilon_2 = 1$ (e.g., InGaAs or Si in the near IR). The air-hole structure was selected because its connectivity promotes large PBGs for TE polarization [27], and TE polarization is required to observe the slot-effect [1]. Compared with a periodic air-hole waveguide, the addition of the slot effectively reduces the dielectric contrast of the 1-D periodic structure. Despite this reduced contrast, large PBGs are observed, with gap-to-midgap ratios $\Delta\omega/\omega_0 = 2(\omega_2 - \omega_1)/(\omega_2 + \omega_1)$ typically around 0.15. As shown in the inset to Fig. 1(a), adjusting

the slot-width *ws* or the hole-radius *r*, influences the gap-to-midgap ratio. For moderate values of *ws*, such as those examined in Fig. 1(a), the gap-to-midgap ratio tends to increase with hole-radius. Here, we note that a mode-gap cavity could theoretically be implemented in a manner similar to other slotted 2-D photonic crystal slab structures where a local modification in the hole size and/or positioning, or alternatively the slot width, give rise to a cavity mode. Recent work has demonstrated the possibility of achieving ultrahigh Q-factors, up to $\sim 7.2–7.5 \times 10^5$, in 1-D mode gap cavities based on a nonslotted air-hole waveguides [28]–[30]; similar Q-factors can be expected for pinch waveguides with proper design optimization. We further discuss such defect modes in Section III.

Immediately above and below the PBG are the *air* and *dielectric bands*, respectively. The *air band* is characterized by the electric fields concentrating primarily in the vicinity of the air-holes (or low index). The fields are also highly evanescent, suggesting that such modes have a very low modal index n_{eff}. If we consider a pinch waveguide operating at 1550 nm, for example, with $r = 0.45a$, $ws = 0.24a$, $w = 1.2a$, and $a = 600$ nm, we find a very low modal index of $n_{eff} \approx 1.16$. Given these characteristics, we expect that such a structure would be particularly well suited for optical sensing in gas or liquid environments, where significant field overlap with cladding materials provides enhanced sensitivity [2]. Furthermore, we predict that this structure could provide substantial enhancements to surface sensing, for example, the detection of biomolecular monolayers, owing to the increase in surface area compared to the traditional slot waveguide [31].

The *dielectric band*, which will serve as our primary focus for the remainder of this study, is characterized by the electric field being very tightly confined to the slot region between air-holes, as shown in the field distribution in Fig. 1(c). This local confinement is a direct result of combining two important effects resulting from Maxwell's equations. The first effect provides strong optical confinement in the *y*-direction, and is the well-known slot-effect resulting from the continuity of the displacement field normal to an interface [1]. For high dielectric contrast structures, this leads to a distinct discontinuity in the electric field in the form of an enhancement in the region of low dielectric constant, as described by (1), where the slot has dielectric constant ε_2 and is oriented such that the *y*-direction is normal to the dielectric interface. Thus, for a large dielectric contrast structure, such as $\varepsilon_1 = 13$, $\varepsilon_2 = 1$, the electric field immediately inside the slot can be enhanced approximately one order of magnitude

$$\mathrm{D}_{y,\varepsilon_1} = \mathrm{D}_{y,\varepsilon_2} \rightarrow \frac{\varepsilon_1}{\varepsilon_2}\mathrm{E}_{y,\varepsilon_1} = \mathrm{E}_{y,\varepsilon_2}. \tag{1}$$

The second effect arises from the periodicity of the structure, resulting in a redistribution of the fields in the *x*-direction, and locally enhances the fields in the regions between holes where the effective dielectric constant is the highest. The tendency for electric fields to concentrate in regions of higher effective dielectric constant can be considered as a property of the electromagnetic variational theorem [17], which states that the lowest frequency mode corresponds to a field distribution that minimizes the electromagnetic energy functional

$$U_f(\mathrm{H}) = \frac{\int d^3\mathrm{r}|\nabla \times \mathrm{E}(\mathrm{r})|^2}{\int d^3\mathrm{r}\varepsilon(\mathrm{r})|\mathrm{E}(\mathrm{r})|^2}. \tag{2}$$

In this expression, H represents the magnetic-field eigenmode that minimizes the electromagnetic energy functional U_f, ε is the dielectric function, and E is the corresponding electric field distribution, subject to $\nabla \cdot \varepsilon \mathrm{E} = 0$. Note that concentrating the electric field to regions of higher dielectric constant helps to minimize U_f by maximizing the denominator of (2). Due to the *dielectric band* containing the lowest frequency modes, the resulting field distributions for this band are most tightly confined to the higher ε regions between air-holes [see Fig. 1(c)] [17].

In Fig. 2, we compare the modal characteristics of the pinch waveguide with those of the traditional slot waveguide and 1-D periodic air-hole waveguide. Individually, the field distributions of the slot waveguide and air-hole waveguide directly illustrate the two primary effects discussed above, which respectively contribute to the strong field confinement observed in the pinch waveguide structure. As expected, the slot waveguide is characterized by strong field confinement

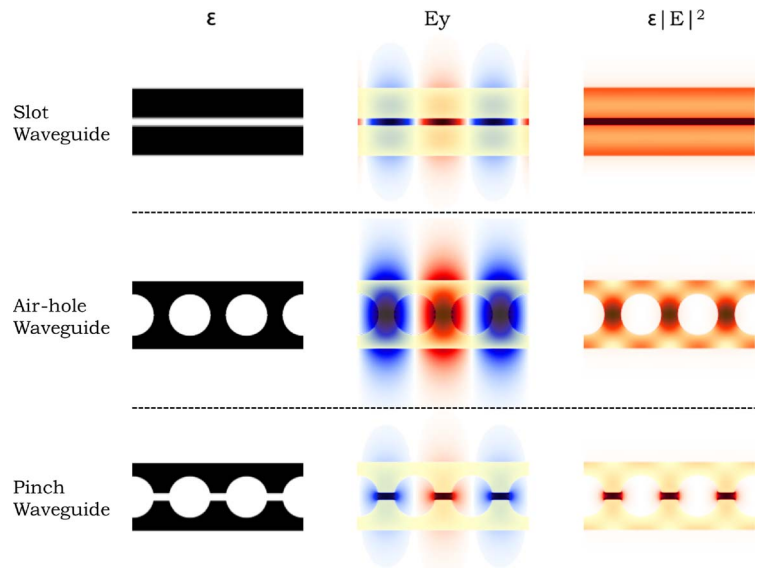

Fig. 2. Example electric field (instantaneous) and power distributions (time-averaged) for three waveguide structures. The pinch waveguide combines principles from both slot and periodic geometries to obtain extreme subwavelength confinement in a guided mode. Note that each field image is normalized to its own linear color scale (dark red + to dark blue −).

in the *y*-direction. However, we note that the time-averaged power density shows a significant fraction of the total power is distributed in the high dielectric region, which is also true for traditional slot waveguides. Typically, a traditional slot waveguide cannot confine more than ∼30% of the optical power inside of the slot region [1]. The air-hole waveguide, by comparison, shows relatively poor confinement in the *y*-direction but strong field localization along the *x*-direction in the region between air-holes, which is especially apparent in the time-average power distribution. This is a primary example of the sort of behavior that is expected from the electromagnetic variational theorem and (2). The combination of the slot effect and the periodic field concentration in the pinch waveguide locally compresses the electric field in space, resulting in a very strong subwavelength confinement and strong localized field enhancements.

2.2. Field Enhancements and Power Confinement

For a more detailed examination, we compare example slot and pinch waveguides with a high dielectric contrast $(\varepsilon_1 = 13, \varepsilon_2 = 1)$, which is designed to operate at $\lambda = 1550$ nm. Choosing $a = 387.5$ nm places the nominal operating range well into the *dielectric band* and away from the band edge where group velocity theoretically slows to zero. This design choice allows us to demonstrate that the fundamental field enhancement of the pinch waveguide is not a slow-light effect, while we note that designing the pinch waveguide to operate in the slow-light regime would only further enhance the local field intensities. Now let us consider a slot width $ws = 0.12a$ of approximately 45 nm. This relatively small slot width is first chosen because for a traditional slot waveguide, the field-enhancement within the slot always increases with reducing slot width [1], and second, it is close to the low-end of the scale of what can be reliably produced by conventional electron-beam lithography. In other words, this choice of *ws* represents a case where the field-intensity in the traditional slot waveguide is very high. We note that for some applications, for example when maximum field enhancement is desired, the optimal design choice may be dictated by technological limitations.

In Fig. 3, we compare the electric field enhancement and power confinement provided by the pinch waveguide with that of the traditional slot waveguide. In order to make this comparison, all intensities are normalized to the total optical power in the respective waveguide and then weighed

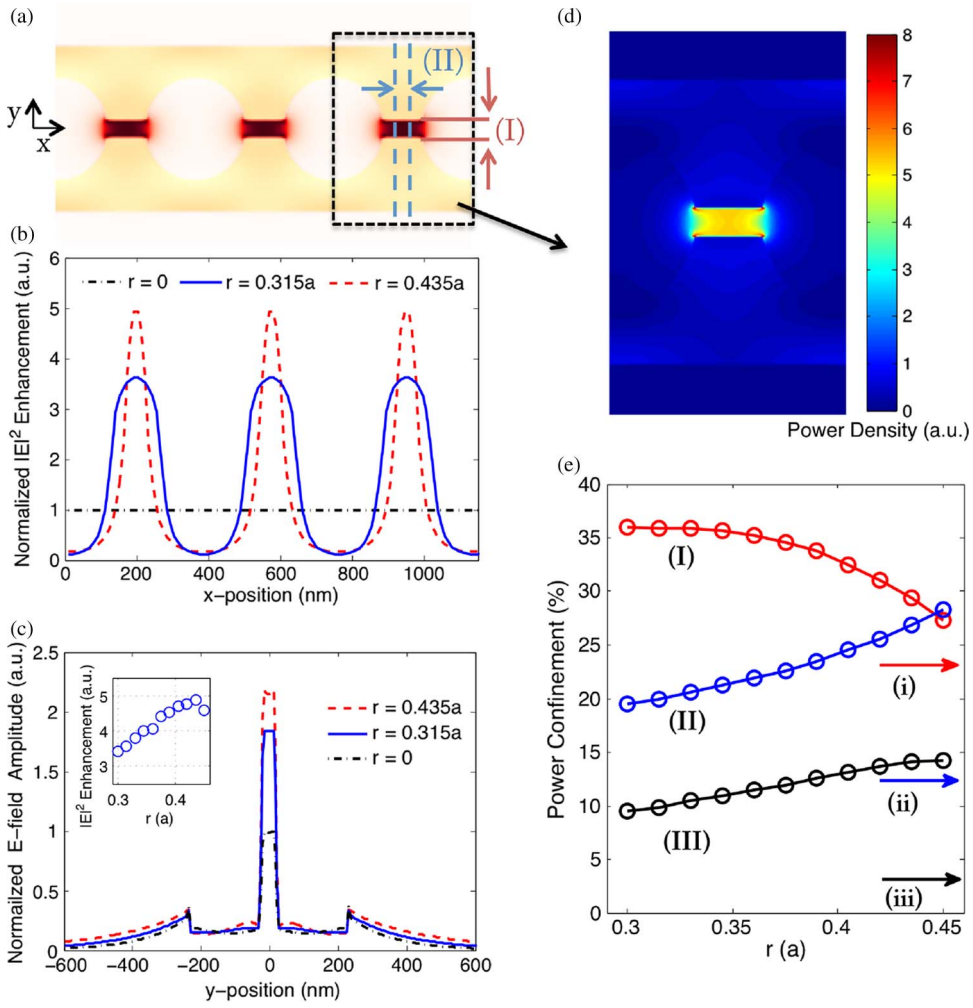

Fig. 3. (a) Example of a pinch waveguide power distribution and illustration of regions (I, II), where power confinement is analyzed in (e). (b) Time-averaged $|E|^2$ enhancement relative to a traditional slot waveguide operating at $\lambda = 1.55$ μm, with $a = 387.5$ nm (slice centered at $y = 0$). (c) Time-averaged E-field amplitude (slice centered between holes), inset circles: simulated peak $|E|^2$ enhancement, along $y = 0$, as a function of hole radius; inset line: the function $1/(1 - 2r)$. (d) Snap shot for $r = 0.36a$ of an animation showing the power density variation with hole-size (Media 1, available for download at http://ieeexplore.ieee.org). (e) Percentage of total power confined to selected regions of the pinch waveguide with $ws = 0.12a$, $w = 1.2a$, and frequency $= 0.25$. Region III is defined as the intersection of regions I and II. Lower case arrows, labeled i–iii, indicate the power confinement of a traditional slot waveguide with the same dimensions.

relative to the traditional slot waveguide. As observed in Fig. 2, the time average of $|E|^2$ is nonzero and, for the traditional slot waveguide, constant as a function of x-position. This is also clear in Fig. 3(b) when examining the field in the middle of the waveguide as a function of x-position for the case $r = 0$ (traditional slot waveguide), where we find a uniform $|E|^2$. The pinch waveguide however, shows significant $|E|^2$ enhancements, up to $\sim$4–5 times greater than the slot waveguide, which are maximized periodically in x at locations directly between holes.

Importantly, we find that both the nominal peak enhancement and the general shape of the spatial enhancement can be tuned by varying the hole radius. As the hole radius is increased, the length of the high index region between holes is reduced. This further compresses the field in the x-direction and results in additional field enhancement [see Fig. 3(b)–(d) and the supplementary video Media 1]. This will be available at http://ieeexplore.ieee.org. The trend for field enhancement as a function of hole radius is shown as the inset to Fig. 3(c). If we assumed that all of the electromagnetic energy was

uniformly confined between holes, then the field enhancement would continue to increase with r, eventually approaching infinity as the hole radius approached $0.5a$. However, this is clearly not the case, as we do not observe an asymptotic increase in the field enhancement. Instead, we find that the field enhancement increases monotonically and plateaus to a maximum value near $r = 0.5a$.

Here, we would like to emphasize that by achieving such strong field enhancements over the traditional slot waveguide, the pinch waveguide achieves normalized field intensities that are superior to any dielectric-based guided mode structure that is not operating in the slow light regime. Also, these field enhancements coincide with a reduced total interaction volume, similar to the tradeoff posed by the traditional slot-waveguide, where the largest enhancements occur for the smallest slot widths.

As shown in Fig. 3(e) we have also investigated the power confinement within particular regions of the pinch waveguide as a function of hole size (again considering $a = 387.5$ nm, $\lambda = 1550$ nm). For this analysis, we define two regions from the unit cell, i.e., regions I and II, each with width $ws = 0.12a$ [see Fig. 3(a)]. We also define a third region, region III, as the intersection of regions I and II, containing a small area $ws \times ws$. The equivalent regions on the traditional slot waveguide are denoted in lower case (i, ii, iii).

Examining the power distribution in the x-direction, we find that up to $\sim$28% of the optical power can be found in region II (centered between air-holes). This is a significant increase over the 12% of power that would be found in the same region ii for any traditional waveguide (slot or otherwise) that has continuous translational symmetry. We find that up to $\sim$35% of the optical power is confined in the y-direction to region I. This value is also larger than the $\sim$23% power confinement that can be achieved in a traditional slot waveguide of the same dimensions. Owing to the behavior observed in Fig. 3(d), we refer to region III as the "pinch" region. The power confined in this region is as high as $\sim$15%, a significant increase over what is found in the traditional slot waveguide, which shows only $\sim$3% power confinement. In other words, the typical power confined within the "pinch" region of the pinch waveguide is up to 400% enhanced compared with a traditional slot waveguide of the same dimensions.

3. FDTD Simulation of a Pinch Nanocavity

To this point, we have focused primarily on the guided mode behavior of the pinch waveguide structure, which requires operating outside the PBG. Importantly however, we can also engineer defect modes within the bandgap by breaking the translational symmetry of the periodic lattice to form a nanocavity [27]–[30]. In Fig. 4, we present an example nanocavity based on the pinch waveguide. The nanocavity consists of three sections: a defect, taper, and Bragg mirror. The taper is an important component as it helps to reduce scattering losses at the otherwise abrupt defect-mirror interface, where there is typically a large mismatch between the effective index of the defect and the evanescent Bloch mode in the mirror [28]–[30], [32]–[34]. Our taper consists of five holes, each with subsequently decreasing radii r_n and lattice constant a_n. Without performing any taper optimization, we have chosen a linear taper, varying a_n from a to $0.85a$, and varying r_n linearly from r to $0.785r$. In this 3-D example, we also utilize a defect spacing $d = 0.825a$, $ws = 0.12a$, $r = 0.42a$, and $w = 1.2a$, and a waveguide height $h = 0.6a$. This combination of slot width and nominal hole radius are selected to produce a large PBG [see Fig. 1(a)]. Finally, we note that while ws is constant throughout this structure, it could be modified locally to serve as an additional tool toward optimizing the taper, cavity, or in customizing the field profile.

Our pinch nanocavity was simulated using the 3-D FDTD method with a grid resolution $a/36$ and subpixel averaging enabled. The defect mode presented by this particular cavity exhibits a very distinct field distribution, as shown in Fig. 4. In particular, we note that similar to our observations for dielectric band guided modes, the electric field amplitude is locally maximized in the "pinch" regions between air-holes. Similar to most slotted cavity designs, the fields are very strongly localized in the y-direction. This results in a very low mode-volume V_{eff}, as defined elsewhere [18], [22], which is determined by 3-D FDTD calculations to be $0.035(\lambda/\mathrm{n})^3$. This value is well below the diffraction limit and dramatically smaller than values reported for nonslotted cavity structures [19], [28]–[30], [33]

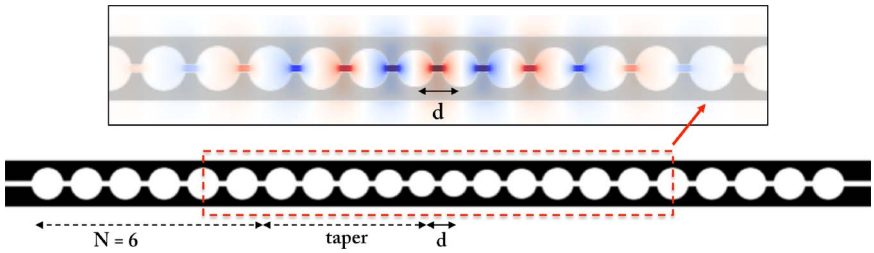

Fig. 4. Slotted nanocavity based on the pinch waveguide structure and the cavity mode Ey distribution. The center-to-center hole spacing is linearly tapered from a to $0.85a$, while the hole radii are linearly tapered from r to $0.785r$. With a defect spacing $d = 0.825a$ and $r = 0.42a$, this structure exhibits a quality factor $Q = 1.56 \times 10^4$ and mode volume $V_{eff} \sim 0.035(\lambda/n)^3$.

and is comparable with what has been reported for slotted 2-D photonic crystal slab modes [22]. This cavity mode also exhibits a high quality factor $Q = 1.56 \times 10^4$. Despite potential for optimization, this Q-factor is among the highest reported for any slotted 1-D photonic crystal cavity [18], [19], [34]. While slotted 2-D photonic crystal slabs have shown theoretical quality factors on the order of 10^5 [5], [22], we note that recent optimizations of nonslotted 1-D cavities have produced ultrahigh theoretical quality factors $\sim 10^7$–10^9 [28], [30], suggesting that simpler 1-D structures can rival the figures of merit set by 2-D photonic crystal slab cavities [35]. Furthermore, we note that the "pinch" geometry offers the potential to dramatically manipulate the localized field confinement and optical gradients [e.g., Fig. 3(d)], which is not directly possible in 2-D photonic crystal slab structures.

4. Outlook

Given the unique properties of the pinch waveguide, we foresee a variety of potential applications. One prospect is for optical manipulation, where small matter, such as nanoparticles or biomolecules, are confined and transported by optical command. One problem faced by conventional optical manipulation techniques, such as optical tweezers or evanescent trapping, is that small particles only interact with a very small fraction of the optical field. This ultimately makes it difficult to achieve sufficiently strong optical forces to manipulate very small particles. Recent advancements have demonstrated increased optical control by using slot waveguides [14], microring resonators [36], and nanocavities [37]. These approaches increase light–matter interaction and correspondingly increase the optical forces experienced by small particles, resulting in unparalleled trapping stiffness [38]. In a similar manner, we expect that the field enhancements and sharp optical gradients of the pinch waveguide could be exploited for optical manipulation, as illustrated in Fig. 5(a). In a guided mode structure, for example, nanoparticles will experience significantly enhanced optical forces owing to the distinct power and electric field concentration in the "pinch" regions. Thus, the structure could be considered as a nanoarray of strong point traps where optical confinement (i.e., Fy, Fz) and radiation pressure (i.e., Fx) are distinctly enhanced. Naturally, a pinch nanocavity, such as the one presented in Section III, could also be employed to further improve the optical confinement and enable stronger stationary trapping.

The strong power confinement of the pinch waveguide further opens the possibility for increasing the effectiveness of integrated active materials. A wide variety of nonlinear [8]–[13] phase changing [39], [40], electroluminescent [41], or otherwise active materials are being explored for achieving optical amplification, modulation, and detection in nanophotonic devices. Integrating these materials into the "pinch" region of the waveguide [see Fig. 5(b)], where power confinement is enhanced $\sim$250–400% over a conventional slot waveguide, could enable more effective and/or compact devices with reduced power requirements. Finally, we propose that pinch waveguides could also be implemented in a variety of geometries, similar to conventional slot waveguides and photonic wires, such as the ring resonator configuration [see Fig. 5(c)]. Depending on the particular application, this structure can be adjusted to operate using either *air band* or *dielectric band* guided

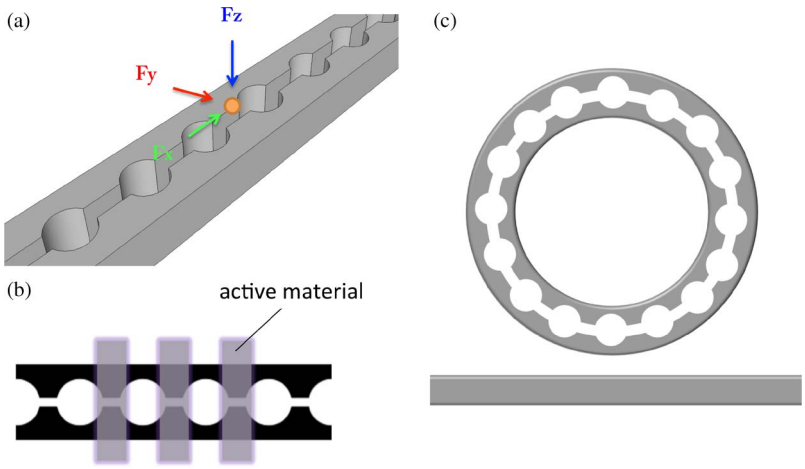

Fig. 5. (a) Pinch waveguide employed for optical nanomanipulation. (b) View of how an active material can be integrated with the pinch waveguide platform. (c) Pinch waveguide in a ring resonator configuration.

modes. Additionally, the field profiles can be fine tuned by modulating the hole and slot sizes, enabling the structure to be further optimized for sensing analytes or manipulating particles of different sizes.

Implementing the pinch waveguide geometry, at optical frequencies, is readily achievable with modern nanofabrication techniques such as electron-beam or nanoimprint lithography followed by reactive ion etching. While the theoretical investigations presented here are for ideal structures, realistic implementations are prone to nonidealities, including distortions to the hole-shape or positioning, as well as sidewall roughness, which can be introduced in the fabrication process. However, the fabrication challenges faced by the pinch waveguide geometry are comparable to those faced by modern photonic crystal and slot waveguide structures. Also, while the field enhancements of the pinch waveguide suggest stronger interaction with sidewall nonidealities and the possibility of greater scattering losses, these interactions are localized periodically, resulting in a reduced total interaction distance. Therefore, we expect the optical losses introduced by sidewall roughness to be comparable with traditional slot waveguides of similar dimensions.

5. Conclusion

We have presented a novel photonic platform, the "*pinch waveguide,*" which is based on a slot waveguide with 1-D periodic holes. The structure exhibits significant localized field enhancements in both guided and defect modes that are stronger than what can be achieved by using either the conventional slot or 1-D periodic hole structures alone. Distinct and tunable optical gradients, as well as localized $|E|^2$ and power confinement enhancements, up to ~4–5 times and ~250–400% enhanced, respectively, over comparable slot waveguides, can be achieved. Notably, the guided mode field enhancements of the pinch waveguide are fundamentally not linked to slow-light effects, as are other previous combinations of slotted and photonic crystal geometries. Therefore, extension into the slow-light regime would only produce further enhancements owing to the reduction in v_g. Importantly, we have also demonstrated that the pinch waveguide can be implemented to construct resonators with ultralow modal volumes and high quality factors, which are more compact and simpler to implement than other 2-D photonic crystal configurations. The pinched field phenomenon arises from the combination of two important results of Maxwell's equations: 1) the slot effect and 2) the electromagnetic variational principle. Many potential applications related to sensing, optical manipulation, and nonlinear or active material integration could benefit from utilizing the pinch waveguide design.

Acknowledgment

J. D. R. acknowledges support from a National Science Foundation Graduate Research Fellowship.

References

[1] V. R. Almeida, Q. Xu, C. A. Barrios, and M. Lipson, "Guiding and confining light in void nanostructure," *Opt. Lett.*, vol. 29, no. 11, pp. 1209–1211, Jun. 2004.
[2] F. Dell'Olio and V. M. Passaro, "Optical sensing by optimized silicon slot waveguides," *Opt. Express*, vol. 15, no. 8, pp. 4977–4993, Apr. 2007.
[3] C. A. Barrios, K. B. Gylfason, B. Sánchez, A. Griol, H. Sohlström, M. Holgado, and R. Casquel, "Slot-waveguide biochemical sensor," *Opt. Lett.*, vol. 32, no. 21, pp. 3080–3082, Nov. 2007.
[4] J. T. Robinson, L. Chen, and M. Lipson, "On-chip gas detection in silicon optical microcavities," *Opt. Express*, vol. 16, no. 6, pp. 4296–4301, Mar. 2008.
[5] A. Di Falco, L. O'Faolain, and T. F. Krauss, "Chemical sensing in slotted photonic crystal heterostructure cavities," *Appl. Phys. Lett.*, vol. 94, no. 6, p. 063 503, Feb. 2009.
[6] Y. Li, J. Zheng, J. Gao, J. Shu, M. S. Aras, and C. W. Wong, "Design of dispersive optomechanical coupling and cooling in ultrahigh-Q/V slot-type photonic crystal cavities," *Opt. Express*, vol. 18, no. 23, pp. 23 844–23 856, Nov. 2010.
[7] M. Li, W. H. P. Pernice, and H. X. Tang, "Ultrahigh-frequency nano-optomechanical resonators in slot waveguide ring cavities," *Appl. Phys. Lett.*, vol. 97, no. 18, p. 183 110, Nov. 2010.
[8] C. Koos, L. Jacome, C. Poulton, J. Leuthold, and W. Freude, "Nonlinear silicon-on-insulator waveguides for all-optical signal processing," *Opt. Express*, vol. 15, no. 10, pp. 5976–5990, May 2007.
[9] T. Vallaitis, S. Bogatscher, L. Alloatti, P. Dumon, R. Baets, M. L. Scimeca, I. Biaggio, F. Diederich, C. Koos, W. Freude, and J. Leuthold, "Optical properties of highly nonlinear silicon-organic hybrid (SOH) waveguide geometries," *Opt. Express*, vol. 17, no. 20, pp. 17 357–17 368, Sep. 2009.
[10] J.-M. Brosi, C. Koos, L. C. Adreani, M. Waldow, J. Leuthold, and W. Freude, "High-speed low-voltage electro-optic modulator with a polymer-infiltrated silicon photonic crystal waveguide," *Opt. Express*, vol. 16, no. 6, pp. 4177–4191, Mar. 2008.
[11] T. Baehr-Jones, M. Hochberg, G. Wang, R. Lawson, Y. Liao, P. A. Sullivan, L. Dalton, A. K.-Y. Jen, and A. Scherer, "Optical modulation and detection in slotted silicon waveguides," *Opt. Express*, vol. 13, no. 14, pp. 5216–5226, Jul. 2005.
[12] C. Koos, P. Vorreau, T. Vallaitis, P. Dumon, W. Bogaerts, R. Baets, B. Esembeson, I. Biaggio, T. Michinobu, F. Diederich, W. Freude, and J. Leuthold, "All-optical high-speed signal processing with silicon-organic hybrid slot waveguides," *Nat. Photon.*, vol. 3, no. 4, pp. 216–219, Apr. 2009.
[13] J. Wülbern, J. Hampe, A. Petrov, M. Eich, J. Luo, A. Jen, A. Falco, T. Krauss, and J. Bruns, "Electro-optic modulation in slotted resonant photonic crystal heterostructures," *Appl. Phys. Lett.*, vol. 94, no. 24, p. 241 107, Jun. 2009.
[14] A. H. J. Yang, S. D. Moore, B. S. Schmidt, M. Klug, M. Lipson, and D. Erickson, "Optical manipulation of nanoparticles and biomolecules in sub-wavelength slot waveguides," *Nature*, vol. 457, no. 7225, pp. 71–75, Jan. 2009.
[15] A. H. J. Yang, T. Lerdsuchatawanich, and D. Erickson, "Forces and transport velocities for a particle in a slot waveguide," *Nano Lett.*, vol. 9, no. 3, pp. 1182–1188, Mar. 2009.
[16] Z. Gaburro, "A design for a photonic syringe with multimode coupled slot waveguides," *Opt. Express*, vol. 18, no. 1, pp. 288–300, Jan. 2010.
[17] J. D. Joannopoulos, S. G. Johnson, J. N. Winn, and R. D. Meade, *Photonic Crystals: Molding the Flow of Light*. Princeton, NJ: Princeton Univ. Press, 2008.
[18] J. T. Robinson, C. Manolatou, L. Chen, and M. Lipson, "Ultrasmall mode volumes in dielectric optical microcavities," *Phys. Rev. Lett.*, vol. 95, no. 14, p. 143 901, Sep. 2005.
[19] A. Gondarenko and M. Lipson, "Low modal volume dipole-like dielectric slab resonator," *Opt. Express*, vol. 16, no. 22, pp. 17 689–17 694, Oct. 2008.
[20] F. Riboli, P. Bettotti, and L. Pavesi, "Band gap characterization and slow light effects in one dimensional photonic crystals based on silicon slot-waveguides," *Opt. Express*, vol. 15, no. 19, pp. 11 769–11 775, Sep. 2007.
[21] T. Yamamoto, M. Notomi, H. Taniyama, E. Kuramochi, Y. Yoshikawa, Y. Torii, and T. Kuga, "Design of a high-Q air-slot cavity based on a width-modulated line-defect in a photonic crystal slab," *Opt. Express*, vol. 16, no. 18, pp. 13 809–13 817, Sep. 2008.
[22] J. Gao, J. F. McMillan, M.-C. Wu, J. Zheng, S. Assefa, and C. W. Wong, "Demonstration of an air-slot mode-gap confined photonic crystal slab nanocavity with ultrasmall mode volumes," *Appl. Phys. Lett.*, vol. 96, no. 5, p. 051 123, Feb. 2010.
[23] A. Taflove and S. C. Hagness, *Computational Electrodynamics: The Finite-Difference Time-Domain Method*. Norwood, MA: Artech House, 2000.
[24] V. A. Mandelshtam and H. S. Taylor, "Harmonic inversion of time signals and its applications," *J. Chem. Phys.*, vol. 107, no. 17, pp. 6756–6769, Nov. 1997.
[25] A. F. Oskooi, D. Roundy, M. Ibanescu, P. Bermel, J. D. Joannopoulos, and S. G. Johnson, "MEEP: A flexible free-software package for electromagnetic simulations by the FDTD method," *Comput. Phys. Commun.*, vol. 181, no. 3, pp. 687–702, Mar. 2010.
[26] A. Farjadpour, D. Roundy, A. Rodriguez, M. Ibanescu, P. Bermel, J. D. Joannopoulos, S. G. Johnson, and G. W. Burr, "Improving accuracy by subpixel smoothing in the finite-difference time domain," *Opt. Lett.*, vol. 31, no. 20, pp. 2972–2974, Oct. 2006.
[27] S. Fan, J. D. Joannopoulos, J. N. Winn, A. Devenyi, J. C. Chen, and R. D. Meade, "Guided and defect modes in periodic dielectric waveguides," *J. Opt. Soc. Amer. B, Opt. Phys.*, vol. 12, no. 7, pp. 1267–1272, Jul. 1995.

[28] P. Deotare, M. McCutcheon, I. Frank, M. Khan, and M. Loncar, "High quality factor photonic crystal nanobeam cavities," *Appl. Phys. Lett.*, vol. 94, no. 12, p. 121 106, Mar. 2009.
[29] A. R. Zain, N. P. Johnson, M. Sorel, and R. M. De La Rue, "Ultra high quality factor one dimensional photonic crystal/photonic wire micro-cavities in silicon-on-insulator (SOI)," *Opt. Express*, vol. 16, no. 16, pp. 12 084–12 089, Aug. 2008.
[30] E. Kuramochi, H. Taniyama, T. Tanabe, K. Kawasaki, Y.-G. Roh, and M. Notomi, "Ultrahigh-Q one-dimensional photonic crystal nanocavities with modulated mode-gap barriers on SiO_2 claddings and on air claddings," *Opt. Express*, vol. 18, no. 15, pp. 15 859–15 869, Jul. 2010.
[31] C. Kang, C. T. Phare, Y. A. Vlasov, S. Assefa, and S. M. Weiss, "Photonic crystal slab sensor with enhanced surface area," *Opt. Express*, vol. 18, no. 26, pp. 27 930–27 937, Dec. 2010.
[32] C. Sauvan, G. Lecamp, P. Lalanne, and J. Hugonin, "Modal-reflectivity enhancement by geometry tuning in photonic crystal microcavities," *Opt. Express*, vol. 13, no. 1, pp. 245–255, Jan. 2005.
[33] M. W. McCutcheon and M. Loncar, "Design of a silicon nitride photonic crystal nanocavity with a quality factor of one million for coupling to a diamond nanocrystal," *Opt. Express*, vol. 16, no. 23, pp. 19 136–19 145, Nov. 2008.
[34] C. Schriever, C. Bohley, and J. Schilling, "Designing the quality factor of infiltrate photonic wire slot microcavities," *Opt. Express*, vol. 18, no. 24, pp. 25 217–25 224, Nov. 2010.
[35] Y. Akahane, T. Asano, B. S. Song, and S. Noda, "High-Q photonic nanocavity in a two-dimensional photonic crystal," *Nature*, vol. 425, no. 6961, pp. 944–947, Oct. 2003.
[36] S. Y. Lin, E. Schonbrun, and K. Crozier, "Optical manipulation with planar silicon microring resonators," *Nano Lett.*, vol. 10, no. 7, pp. 2408–2411, Jul. 2010.
[37] S. Mandal, X. Serey, and D. Erickson, "Nanomanipulation using silicon photonic crystal resonators," *Nano Lett.*, vol. 10, no. 1, pp. 99–104, Jan. 2010.
[38] X. Serey, S. Mandal, and D. Erickson, "Comparison of silicon photonic crystal resonator designs for optical trapping of nanomaterials," *Nanotechnology*, vol. 21, no. 30, p. 305 202, Jul. 2010.
[39] J. Nag, J. D. Ryckman, M. Hertkorn, B. K. Choi, R. F. Haglund, Jr., and S. M. Weiss, "Ultrafast compact silicon-based ring resonator modulators using metal-insulator switching of vanadium dioxide," *Proc. SPIE*, vol. 7597, p. 759 710, 2010.
[40] R. M. Briggs, I. M. Pryce, and H. A. Atwater, "Compact silicon photonic waveguide modulator based on the vanadium dioxide metal-insulator phase transition," *Opt. Express*, vol. 18, no. 11, pp. 11 192–11 201, May 2010.
[41] C. A. Barrios and M. Lipson, "Electrically driven silicon resonant light emitting device based on slot-waveguide," *Opt. Express*, vol. 13, no. 25, pp. 10 092–10 101, Dec. 2005.